


Article

Seismic Upgrade of an Existing Reinforced Concrete Building Using Steel Plate Shear Walls (SPSW)

Niki Balkamou and George Papagiannopoulos * 

Laboratory of Structural Engineering and Applied Mechanics, Hellenic Open University, 26335 Patras, Greece; nickybalkamou@gmail.com

* Correspondence: papagiannopoulos@eap.gr

Abstract: Steel Plate Shear Walls (SPSW) provide significant lateral load capacity and can be utilized in the seismic retrofit and upgrade of existing reinforced concrete (r/c) buildings. In this study, the application of SPSW to retrofit a r/c building designed according to older seismic provisions is presented. Three different options to model SPSW are utilized, i.e., by equivalent braces, by finite elements, and by membrane elements, seeking not only to appropriately simulate the actual behavior of the SPSW but also to achieve the desired seismic behavior of the retrofitted building. Specific seismic response indices, including plastic hinge formations, are derived by non-linear time-history analyses in order to assess the seismic behavior of the retrofitted r/c building. Inspection of the results provided by non-linear analyses in conjunction with the different modeling options of the SPSW leads to the conclusion that the model with the membrane elements exhibits the best performance, implying that for the seismic retrofit and upgrade of existing r/c buildings, the use of membrane elements to model the SPSW is recommended.

Keywords: steel plate shear walls (SPSW); reinforced concrete building; equivalent brace model; finite element model; orthotropic membrane model; nonlinear time-history analysis



Citation: Balkamou, N.; Papagiannopoulos, G. Seismic Upgrade of an Existing Reinforced Concrete Building Using Steel Plate Shear Walls (SPSW). *Appl. Sci.* **2024**, *14*, 443. <https://doi.org/10.3390/app14010443>

Academic Editor: Maria Favvata

Received: 7 December 2023

Revised: 30 December 2023

Accepted: 30 December 2023

Published: 3 January 2024



Copyright: © 2024 by the authors. Licensee MDPI, Basel, Switzerland. This article is an open access article distributed under the terms and conditions of the Creative Commons Attribution (CC BY) license (<https://creativecommons.org/licenses/by/4.0/>).

1. Introduction

The majority of reinforced concrete (r/c) buildings in Greece, for residential, office, and other purposes, were constructed before 1985, and their seismic design was performed on the basis of the 1959 Greek Seismic Code [1]. These r/c buildings normally do not possess the desirable characteristics that modern seismic codes envisage through the application of certain design criteria. Consequently, these r/c buildings are considered susceptible to seismic damages or failures and necessitate an in-depth evaluation in order to assess the feasibility of their possible seismic retrofit and upgrade.

The methods used in seismic retrofit and upgrade of existing r/c buildings in Greece and elsewhere are described in detail in [2] and commonly involve r/c and FRP (fiber-reinforced polymer) jacketing, r/c shear walls, strengthening of infill panels and steel braces, as well as the mature technologies of base isolation and added damping devices. Despite the versatility and diversity of the seismic retrofit options offered by steel elements, it seems that their use has been restricted to steel braces, usually positioned in a concentric (diagonal or cross-diagonal) manner with respect to a r/c frame, whereas steel jackets and plates have been almost totally substituted by FRP materials [2].

It is true that modern seismic codes, e.g., [3], do not promote specific steel elements for the seismic retrofit and upgrade of existing r/c buildings. The reason is that extensive numerical and experimental data that certify the benefits behind the use of many novel steel elements in seismic retrofits and upgrades of existing r/c buildings became available after the initiation of such codes. The most representative example of such steel elements is the buckling-restrained brace [4–8], even though other steel systems have also evolved or seem to have potential [9–12].

A steel element of special interest for the seismic retrofit and upgrade of existing r/c buildings is the Steel Plate Shear Wall (SPSW). The use of SPSW in steel structures as a lateral force-resisting system enjoys popularity in several countries, e.g., Japan, Mexico, Canada, and the U.S.A., and detailed design criteria are available in ANSI/AISC 341-22 [13] and CSA S16-19 [14] design standards. With respect to the application of SPSW in the seismic retrofit of existing r/c buildings, to the best of the authors' knowledge, one can consult [15–17]. Among the various numerical and experimental works dealing with the seismic retrofit and upgrade of r/c buildings with SPSW, one can name those in [18–23]. A key issue with respect to the anticipated seismic performance of a retrofitted SPSW r/c building is the interaction achieved between the steel and the existing r/c system, i.e., the actual forces transferred between the two materials.

A typical SPSW system, shown in Figure 1, consists of a thin steel web-plate with a common thickness ranging from 5 to 25 mm, two boundary columns, and horizontal boundary beams [17]. The boundary columns are called vertical boundary elements (VBE), and the beams are called horizontal boundary elements (HBE). With respect to terminology, in steel structures, the term SPSW is used if standard steel sections are employed as HBEs and VBEs. However, when referring to a r/c frame, two configurations can be accomplished: (i) in the first one, a metal sheet or plate is inserted between the existent r/c beams and columns that essentially play the role of the HBEs and the VBEs; (ii) in the second one, the steel plate is inserted between added steel columns (HBEs), implying that the resulting SPSW does not occupy the entire bay span of the r/c frame. Taking into account the relevant literature for both configurations (i) and (ii) studied in the following, it is decided for reasons of uniformity to keep the term SPSW.

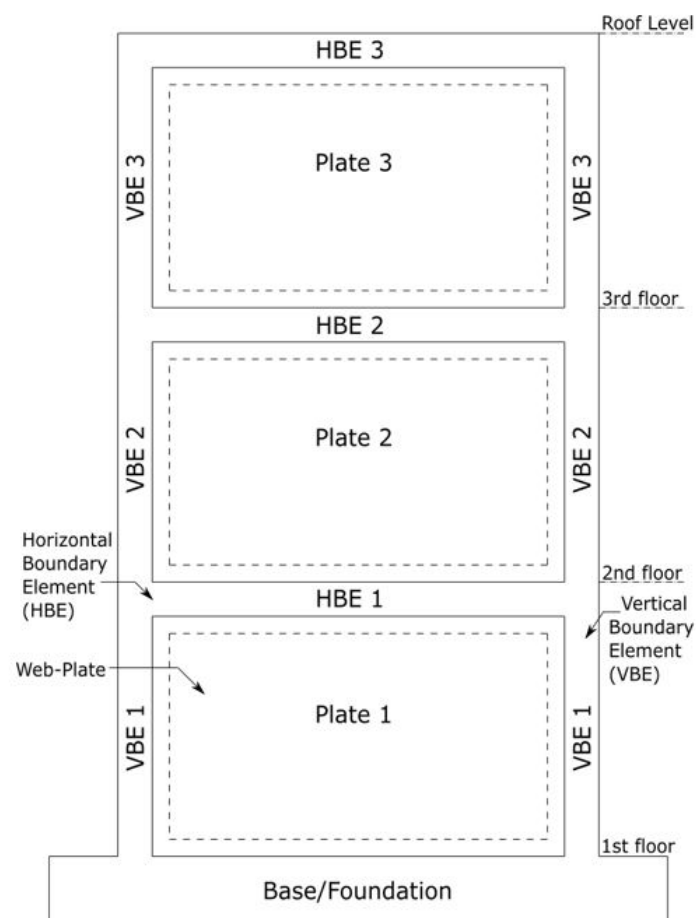


Figure 1. Elements of a typical SPSW for a 3-story.

The strength of the connection of the SPSW with the surrounding members has to be greater than the strength of the SPSW itself. This way, the SPSW yields before yielding of the surrounding members occurs. The steel plate can be stiffened or unstiffened. To reduce the slenderness of the steel plate, stiffeners are added in a vertical or horizontal configuration, even in some cases in a diagonal manner, providing, thus, the buckling strength needed to allow shear yielding of the plate.

The mechanics of a stiffened or unstiffened SPSW are described in [17], revealing the development of a tension field in the plate as the main mechanical characteristic. Unstiffened SPSWs are capable of resisting seismic loads by developing a diagonal tension field with an optimum inclination angle of $\alpha = 45^\circ$. In slender unstiffened SPSWs, the tension field is formed after the buckling of the plate but before its shear yielding, whereas in stiffened SPSWs, the plate yields and then buckles. However, depending on the spacing and thickness of the stiffeners, the tension-field action in stiffened SPSW may take place when buckling occurs and before shear yielding [17].

SPSWs do not significantly increase the mass of the structure and can be easily replaced in case of failure. Moreover, their erection process is faster and easier than with other conventional retrofitting techniques [24]. From the perspective of capacity design [25], the HBEs (beams) should resist the demands of the tension field yielding of the steel plate, and the VBEs (columns) should resist the demands of the tension field yielding and flexural yielding of the HBEs. Therefore, it is important that the boundary elements have adequate strength and stiffness to ensure the full development of the tension field.

Retrofit of r/c buildings is a highly active research domain and covers several hazard scenarios such as fire, seismic events, and explosions, e.g., [26–28]. Attempting to remobilize the interest of practicing engineers and researchers regarding the application of SPSW for seismic retrofit and upgrade purposes, this paper investigates the effectiveness of the SPSW on an existing r/c building designed by older seismic provisions. In particular, expanding the knowledge gained by previous works in the field [18–23], what this present study seeks to make clear is how the modeling and configuration of the SPSW have an impact on the desired seismic performance of the existing r/c building. To be sure in capturing the effects of modeling and configuration of SPSW, three-dimensional non-linear time-history (NLTH) analyses are conducted, thus, from a computational point of view, the best option available for seismic response purposes is selected. On the basis of specific seismic response results obtained by NLTH analyses, including plastic hinge formations, and letting aside any issues related to fabrication and cost, conclusions about the modeling, configuration, and effectiveness of the SPSW for r/c buildings similar to the type studied herein are drawn.

2. Description of the r/c Building

The r/c building under study is a 3-story building located in Amaliada, Greece, and its design was carried out in 1976 on the basis of the requirements of the 1959 seismic code [1]. A common characteristic of r/c buildings designed by this seismic code is their poor ductile behavior and, in many cases, the scarcity of enough transverse (shear) steel reinforcement for columns. Thus, r/c buildings designed according to [1] cannot conform to ductile seismic requirements [2,3] unless a case-dependent seismic upgrade strategy is employed. The whole set of architectural plans and formworks was available at the time of this study and it is indicatively shown in Figures 2–4. According to Figures 2 and 3 and more specifically section AA', the building has an asymmetrical floor plan and a total height of 10.65 m. The first storey is 4.15 m high, while the second and third storeys have a height of 3.25 m each.

The dimensions (in cm) of all beams are 20/50, whereas those of columns are 35/35 for the first storey and 30/30 for the second and third storeys. The longitudinal steel reinforcement of beams and columns is presented in Tables 1 and 2, respectively. It is also noted that the transverse reinforcement is $\Phi 6/220$ (in mm) for beams and $\Phi 8/150$ (in mm) for columns. The thickness of the floor slabs is 14 cm. The material properties and the detailing rules of the building align with the seismic provisions of 1959 [1]. More specifically,

the grades of concrete and steel reinforcement are C12/15 and S220, respectively. With respect to the loads considered for the design of the building, the dead and live loads on the slabs are 0.8 kN/m^2 and 2.0 kN/m^2 , respectively, whereas, for the cantilever slabs, a live load equal to 5.0 kN/m^2 is assumed. The dead loads from infills (9.9 kN/m for the external ones and 5.8 kN/m for the internal ones) are distributed to the beams.

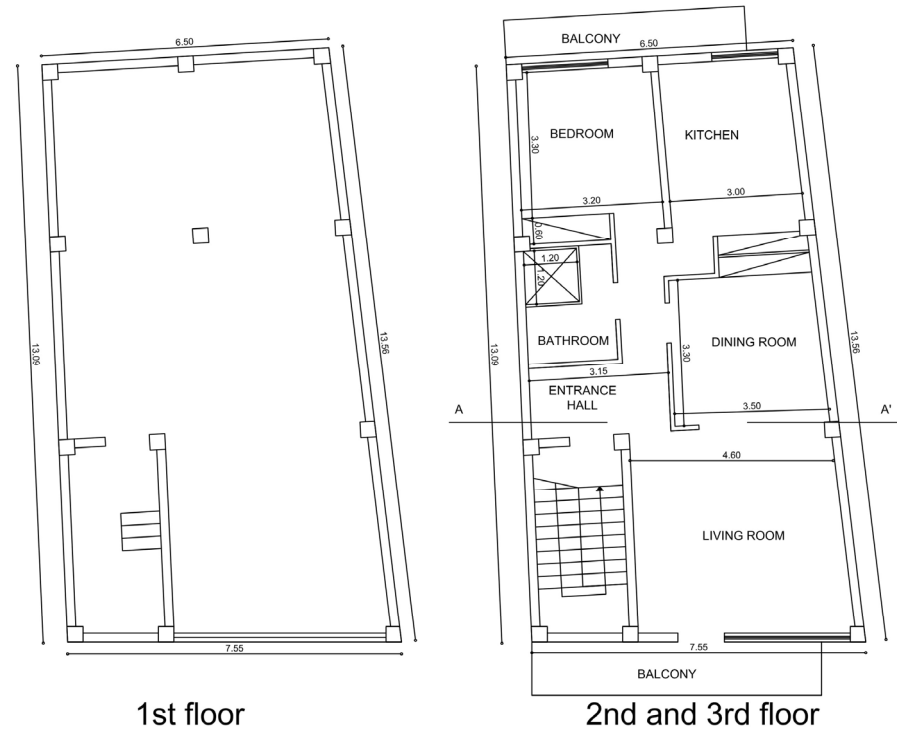


Figure 2. Layout of the r/c building: first (ground) floor (left); second and third floors (right).

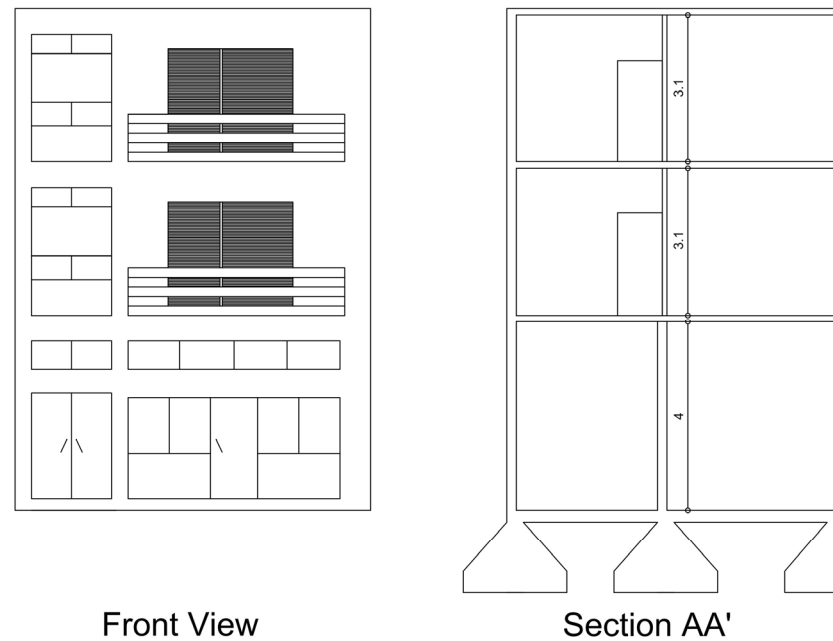
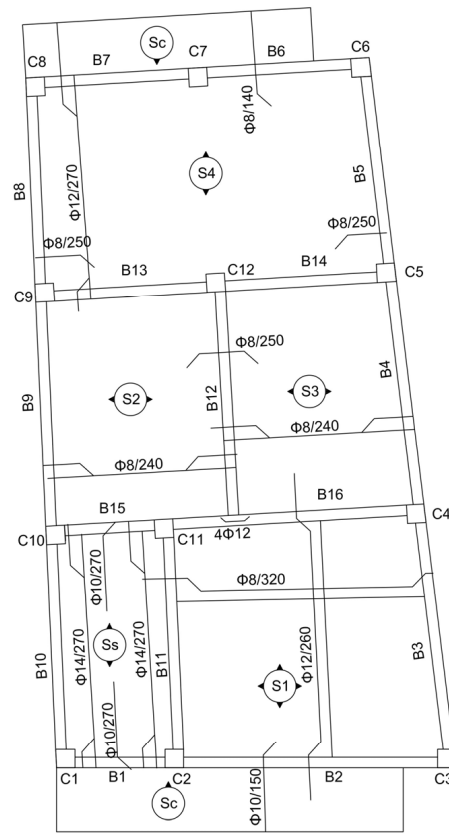


Figure 3. Front view (left) and section (right) of the r/c building.



Formwork of 1st floor

Figure 4. Formwork of 1st floor.

Table 1. Longitudinal reinforcement of beams.

Beams	Span (Bottom)	Support I (Top)	Support II (Top)
B1	4Φ12	2Φ12	4Φ14 + 2Φ12
B2	2Φ18 + 2Φ20	1Φ18 + 1Φ20 + 4Φ14	1Φ18 + 1Φ20
B3	4Φ14	2Φ14	2Φ14
B4	4Φ18	2Φ18	2Φ18
B5	4Φ12	2Φ12	2Φ12
B6	4Φ12	4Φ12	2Φ12
B7	4Φ14	2Φ14	2Φ14 + 2Φ12
B8	4Φ12	2Φ12	2Φ12
B9	4Φ18	2Φ18	2Φ18
B10	4Φ12	2Φ12	2Φ12
B11	4Φ14	2Φ14	2Φ14
B12	2Φ18 + 2Φ20	1Φ12 + 1Φ20	1Φ18 + 1Φ20
B13	4Φ12	2Φ12	2Φ12
B14	4Φ12	2Φ12	2Φ12
B15	4Φ12	2Φ12	4Φ12
B16	5Φ18	2Φ12 + 3Φ18	3Φ18

Table 2. Longitudinal reinforcement of columns.

Column	1st Storey	2nd Storey	3rd Storey
C1	4Φ20	4Φ20	4Φ20
C2	8Φ20	6Φ20	4Φ16
C3	4Φ20	4Φ20	4Φ20
C4	8Φ16	6Φ16	4Φ16

Table 2. Cont.

Column	1st Storey	2nd Storey	3rd Storey
C5	4Φ20	4Φ18	4Φ16
C6	4Φ20	4Φ20	4Φ20
C7	8Φ16	6Φ16	4Φ16
C8	4Φ20	4Φ20	4Φ20
C9	4Φ20	4Φ18	4Φ16
C10	4Φ20	4Φ18	4Φ16
C11	8Φ20	6Φ20	4Φ16
C12	8Φ16	6Φ16	4Φ16

3. Seismic Analysis of the r/c Building

On the basis of the data presented in the previous section, a numerical model of the r/c building was created in SAP 2000 [29], and it is shown in Figure 5. In this model, frame elements are used for beams and columns and shell elements for the floor slabs. Concrete cracking is conservatively taken into account by considering for all members an effective stiffness equal to 50% of the gross stiffness. The position of the staircase is found not to be critical for the seismic response of the r/c building, and, thus, it is not included in the numerical model. Infills are included in the model, but only as loads to the beams. The r/c building is assumed to be fixed-base (base fixity is denoted with green symbols in the figures that follow), and, hence, soil-structure-interaction effects are absent.

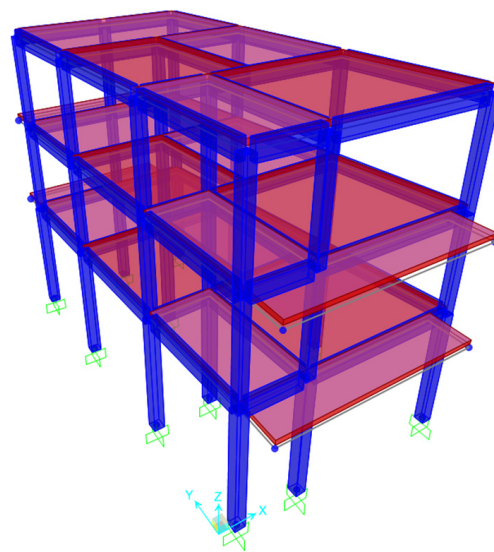


Figure 5. Model of the r/c building.

It is then assumed that the r/c building must resist the seismic load defined by the design spectrum of EC8 [30] for a peak ground acceleration (PGA) equal to 0.24 g (representative of the broader area [31] where the r/c building under study lies), soil class B, importance factor $\gamma = 1.0$, and behavior factor $q = 1.5$. Modal response spectrum analysis of the fixed-base r/c building is performed using the 100–30% spectral combination rule, and the storey shears in both horizontal directions of the building are computed. These storey shears are used for the design of the SPSW in the following and read: 988.113 kN and 926.853 kN for the first storey in the x and y directions, respectively; 729.937 kN and 685.458 kN for the second storey in the x and y directions, respectively; and 292.945 kN and 279.892 kN for the third storey in the x and y directions, respectively. The fundamental period of the r/c building is $T_1 = 0.837$ s.

Next, to identify the potential seismic damage in the critical regions of the beams and columns of the r/c building, NLTH analyses are conducted using three seismic motions for

which their response spectrum is compatible with the aforementioned design spectrum. The two horizontal components of these seismic motions are used interchangeably with respect to the two horizontal axes of the r/c building. Thus, in total, six NLTH analyses are executed assuming: (i) both material and geometrical nonlinearities; (ii) the innate viscous damping of the r/c building to be 3% and the (Rayleigh) damping matrix to be defined using the well-known mass and stiffness proportionality factors; (iii) point plastic hinges at the ends of beams and columns in order to take into account their inelastic behavior. These plastic hinges to beams are formed by bending moments, whereas those to columns are formed by the combination of axial force and bending moments [29,32]. A flexure-shear failure condition is also considered for columns [29,32].

The NLTH analyses revealed almost similar patterns regarding the number of plastic hinge formations on the beams and columns of the r/c building. Figure 6 displays these plastic hinges for the case of the first seismic motion, where one can notice unwanted plastic hinges not only at the top end of the columns of the first storey but also at both ends of the columns of the second storey. Besides the excessive plastic hinge rotation at the bottom end of one column of the first storey, the plastic hinges to the columns of the first two storeys are classified in the IO (Immediate Occupancy)-LS (Life Safety) performance level range according to the acceptance criteria of [32]. In the figures that follow, the legends B, IO, LS, CP, C, etc. are in accordance with the normalized force versus deformation curve of [32]. The maximum values for transient interstorey drift ratios (IDRs), residual interstorey drift ratios (RIDR), and base shear are listed in Table 3. The definition and calculation of IDR, RIDR, and base shear in the context of time-domain seismic analysis are described in [33]. In Table 3, symbols of the form “1a” and “1b” are used to denote the two cases of using the two horizontal components of the first seismic motion interchangeably with respect to the horizontal axes of the building. More specifically, “1a” denotes that the 1st horizontal component of the seismic motion is applied along the x direction of the building and the 2nd horizontal component is applied along the y direction, whereas “1b” denotes the opposite application of these components with respect to the x and y directions of the building.

The maximum RIDR is 1.37%, which is well beyond the maximum allowable value of 0.5% usually considered [34]. According to the results presented in Table 3 and the plastic hinge formation shown in Figure 6, a soft-storey mechanism is anticipated to occur. A retrofit scheme using SPSW is proposed in the next section in order to improve the overall seismic behavior of the r/c building.

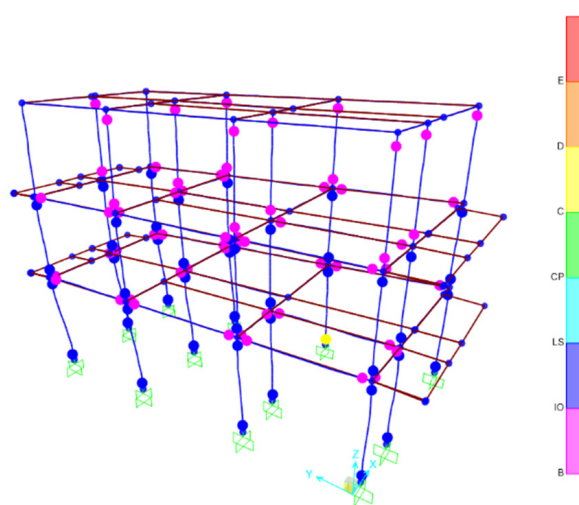


Figure 6. Plastic hinge formations for seismic motion “1b”.

Table 3. Maximum values for IDR, RIDR, and base shear.

Horizontal Direction of the Building	Seismic Motion	Maximum IDR (%)			Base Shear (kN)	Maximum RIDR (%)
		1st Storey	2nd Storey	3rd Storey		
X	1a	1.15	0.51	0.19	507.3	0.69
	1b	2.03	1.06	0.33	557.6	0.70
	2a	1.19	0.58	0.17	464.6	0.61
	2b	1.79	0.52	0.18	471.6	1.37
	3a	0.90	0.53	0.21	422.1	0.37
	3b	1.08	0.53	0.22	580.4	0.26
Y	1a	1.81	1.49	0.37	490.4	0.70
	1b	0.77	0.53	0.29	440.9	0.17
	2a	1.15	0.87	0.26	441.4	0.89
	2b	1.67	0.63	0.21	450.1	1.21
	3a	1.09	0.70	0.26	410.3	0.21
	3b	1.10	0.63	0.24	448.8	0.64

4. Modeling of the SPSWs

The SPSWs are configured only at the external frames of the building and are continuous along its height. Taking into account that three modeling options for SPSWs are provided in [17], NLTH analyses are carried out separately for each modeling option in order to assess its effect on the seismic response of the building. These modeling options are briefly described in the following: It is recalled that the storey shears found by modal response spectrum analyses are used in the design of the SPSWs.

4.1. Equivalent Brace Model (EBM)

Each SPSW is modeled by a diagonal tension-only brace, designed according to [17]. The mechanics behind this model are that a SPSW behaves like a tension-only brace, assuming the inclination angle of the tension field to be $\alpha = 45^\circ$. The thickness of the steel plate is determined according to the following equation [17]

$$t_w \geq \frac{V_u}{0.90 \cdot 0.42 \cdot f_y \cdot L_{cf} \cdot \sin 2\alpha} \quad (1)$$

where L_{cf} is the clear distance between the VBEs (columns), f_y is the yield stress of the steel web-plate (herein considered 235 MPa), and V_u is the shear force taken from the modal response spectrum analysis. The thickness of the SPSW should be specified by the equation [17]

$$\frac{\min(L, h)}{t_w} \leq 25 \sqrt{\frac{E}{F_y}} \quad (2)$$

where L and h are the length and height of the web-plate, respectively, and E is the modulus of elasticity of steel. The resulting thickness is $t_w = 5.0$ mm for each plate. ANSI/AISC 341-22 [13] and CSA S16-19 [14] design standards require that the length-to-height (L/h) ratio of the web-plates satisfy $0.8 < L/h \leq 2.5$. Additionally, the moment of inertia I_c of the VBEs should satisfy the following equation [13,17]

$$I_c \geq \frac{0.00307 \cdot t_w \cdot h^4}{L} \quad (3)$$

Thus, the area A of the equivalent tension brace is calculated by [13]

$$A = \frac{L \cdot t_w \cdot \sin 2\alpha}{2 \cdot \Omega_s \cdot \sin \theta} \quad (4)$$

where θ is the angle between the vertical and longitudinal axes of the equivalent diagonal brace, L is the distance between the centerlines of the VBEs, and $\Omega_s = 1.2$ is the system

overstrength factor. The resulting brace sections are assumed to be of CHS type, and the resulting sections are CHS 273/16 for the first storey and CHS 244.5/16 for the second and third storeys. The model of the r/c building with SPSWs modeled by equivalent braces is shown in Figure 7. The fundamental period of the r/c building in Figure 7 is $T_1 = 0.739$ s.

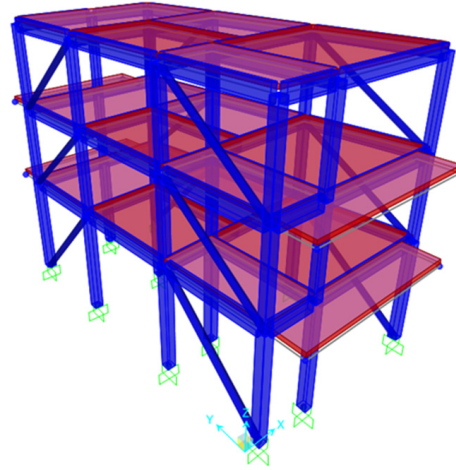


Figure 7. Modeling SPSWs with equivalent braces.

4.2. Finite Element Model (FEM)

Each SPSW is simulated by shell elements. The thickness of the shell elements is that found above by the application of Equations (1) and (2), i.e., $t_w = 5$ mm. This model is shown in Figure 8. The VBEs needed for the SPSW are essentially offered by the r/c columns to which an additional one-sided steel sheet or plate is attached. The fundamental period of the r/c building in Figure 8 is $T_1 = 0.773$ s.

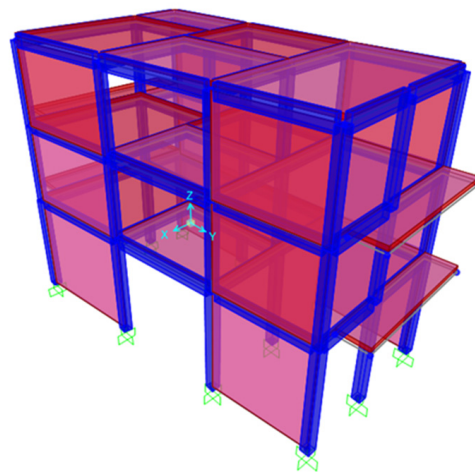


Figure 8. Modeling SPSWs by finite (shell) elements.

An additional configuration of the SPSW is introduced at this point and displayed in Figure 9. This configuration permits the insertion of the SPSWs in both horizontal directions of the building. More specifically, according to Figure 9, the number of SPSWs remains the same, but in comparison to the model shown in Figure 8, SPSWs with smaller dimensions are employed in order not to occupy the entire bay span. This configuration of SPSWs is achieved with the aid of steel columns with flanged profiles. Thus, the web-plates are rigidly connected to HEA180 columns in the first storey and to HEA160 columns in the second and third storeys.

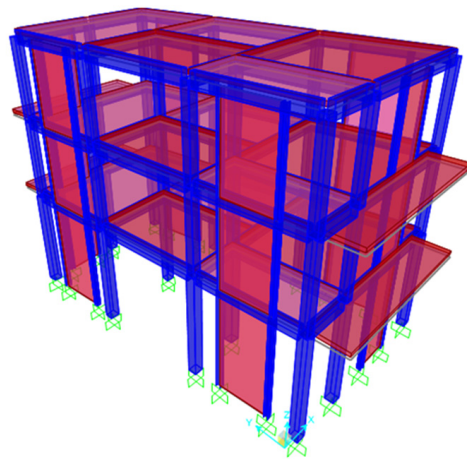


Figure 9. Modeling smaller SPSWs by finite (shell) elements.

The length of the SPSWs is 2.0 m in the y direction and 1.5 m in the x direction. It should be noted that the length-to-height ratio does not satisfy the condition $0.8 < L/h \leq 2.5$ and according to the [14] the use of intermediate stiffeners is suggested. In this case, the required web-plate thickness is determined by the following equation (the shear force V_u is known or can be estimated)

$$V_u = 0.9 \cdot 0.6 \cdot F_y \cdot t_w \cdot L_{cf} \quad (5)$$

The minimum selected thickness is $t_w = 5$ mm for each plate. Stiffeners are ignored in the current study, leading to more conservative results due to the lower stiffness of the plate. The fundamental period of the r/c building in Figure 9 is $T_1 = 0.370$ s.

4.3. Orthotropic Membrane Model (OMM)

The web-plates of the SPSWs shown in Figure 9 are now modeled by membrane elements. To take into account the difference between the tension and compression strength of the web-plates, an orthotropic steel material is considered. The orthotropic membrane model depends on the inclination angle, leading to a reorientation of the local axes of the membrane elements. Therefore, the local axes of the membrane elements are rotated by 45° . Moreover, the stiffness value along the axis that corresponds to the compression diagonal is degraded to 2%, the Poisson ratio is set to $\nu_{12} = 0$, and the shear modulus is set equal to $G = 0$. This way, the assumed tension-field action of the web-plates is adequately represented.

5. Seismic Response Results of the Retrofitted r/c Building

5.1. Equivalent Brace Model (EBM)

The braces resist only tensile axial loads as expected, however, contrary to the desired behavior of the SPSWs, they do not yield. The maximum values for IDRs, RIDRs, and base shear are listed in Table 4 (the symbols “1a”, “1b”, etc. have been previously explained). In comparison to the results presented in Section 3 for the non-retrofitted building, the maximum RIDR is reduced to $0.41\% < 0.50\%$, but the maximum base shear is significantly increased and reaches 1934 kN. Therefore, modeling the SPSWs with EBMs leads to a stiffer building and, thus, to reduced displacements; nevertheless, a soft-storey mechanism is still anticipated to occur. With reference to Figure 10 (plastic hinge excursions for the worst seismic motion “1b”) and on the basis of the acceptance criteria of [29], plastic hinges to columns for all six NLTH analyses performed either remain in the range defined by the IO-LS performance levels or surpass the LS performance level.

Table 4. Maximum values for IDR, RIDR, and base shear.

Horizontal Direction of the Building	Seismic Motion	Maximum IDR (%)			Base Shear (kN)	Maximum RIDR (%)
		1st Storey	2nd Storey	3rd Storey		
X	1a	0.66	0.64	0.40	647.8	0.10
	1b	1.63	1.28	0.28	726.8	0.34
	2a	1.19	0.63	0.27	688.1	0.12
	2b	0.79	0.52	0.32	602.1	0.11
	3a	0.86	0.70	0.39	723.4	0.22
	3b	1.03	0.78	0.35	670.8	0.18
Y	1a	0.15	0.15	0.75	1934	0.41
	1b	0.24	0.19	0.38	1012	0.11
	2a	0.16	0.15	0.40	1318	0.12
	2b	0.14	0.15	0.51	1165	0.24
	3a	0.16	0.17	0.55	1380	0.17
	3b	0.16	0.12	0.45	1147	0.21

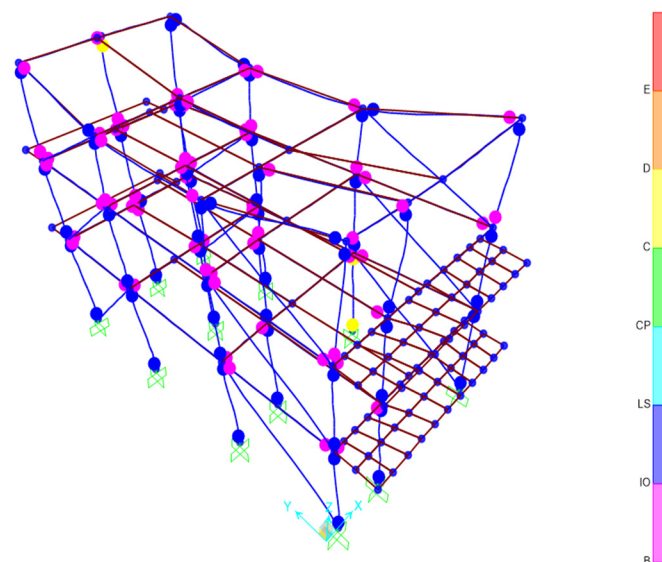


Figure 10. Plastic hinge formations—Equivalent Brace Model (EBM).

5.2. Finite Element Model (FEM)

The results of the retrofitted building shown in Figure 8 are described first. The maximum values for IDRs, RIDR, and base shear are listed in Table 5, and in comparison to the results presented in Section 3 (for the non-retrofitted building) and Section 5.1 (for the retrofitted building–EBM case), the maximum RIDR and base shear are increased to 1.71% > 0.50% and 2680 kN (i.e., by 38.6%), respectively.

Figure 11 displays the worst plastic hinge excursions (coming from the seismic motion “1b”). According to the acceptance criteria of [29], plastic hinges to columns for five NLTH analyses performed remain in the range defined by the IO-LS performance levels, and in one NLTH analysis, they surpass the LS performance level. In general, contrary to the EBM case described in the previous section, modeling of the SPSWs with FEMs (Figure 8) indicates ductile behavior of the building and reveals no or small damage to several beams and columns in almost all NLTH analyses performed. Table 6 presents the Von Mises stresses and the maximum shear stresses of the SPSWs, demonstrating that the SPSWs have not been fully utilized, as none of the plates yielded.

Table 5. Maximum values for IDR, RIDR, and base shear.

Horizontal Direction of the Building	Seismic Motion	Maximum IDR (%)			Base Shear (kN)	Maximum RIDR (%)
		1st Storey	2nd Storey	3rd Storey		
X	1a	0.72	0.67	0.20	626.1	0.09
	1b	2.46	1.22	0.27	647.5	1.71
	2a	1.05	0.73	0.24	604.6	0.13
	2b	1.26	0.48	0.22	534.1	0.54
	3a	0.76	0.76	0.30	735.3	0.09
	3b	0.77	0.85	0.40	723.6	0.15
Y	1a	0.09	0.11	0.07	2680	0.01
	1b	0.32	0.19	0.08	2248	0.21
	2a	0.14	0.11	0.06	2104	0.02
	2b	0.19	0.13	0.08	2406	0.07
	3a	0.13	0.16	0.08	2558	0.01
	3b	0.11	0.14	0.08	2096	0.02

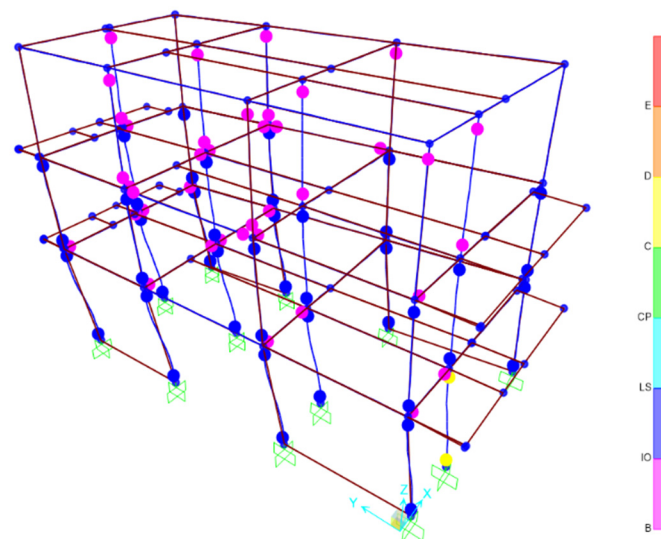


Figure 11. Plastic hinge formations—Finite Element Model (FEM).

Table 6. Maximum Von Mises and shear stress to SPSWs.

Seismic Motion	Von Mises Stress (MPa)	≤235 MPa	Maximum Shear Stress τ_{max} (MPa)	≤235/√3 MPa
1a	44.27	✓	27.58	✓
1b	52.15	✓	21.41	✓
2a	45.92	✓	19.81	✓
2b	42.28	✓	23.54	✓
3a	65.12	✓	24.18	✓
3b	42.63	✓	23.28	✓

The results of the retrofitted building shown in Figure 9 are described next. The maximum values for IDRs, RIDR, and base shear are listed in Table 7, and in comparison to the results presented in Section 3 (for the non-retrofitted building) and the previous model (Figure 8), the maximum RIDR is drastically decreased to 0.036% < 0.5% and the maximum base shear reduces to 2066 kN (i.e., by 23%). The inelastic behavior of the building is improved, and as revealed by the plastic hinge excursions shown in Figure 12 (worst case), plastic hinges to columns for all six NLTH analyses performed remain below the range defined by the LS.

Table 7. Maximum values for IDR, RIDR, and base shear.

Horizontal Direction of the Building	Seismic Motion	Maximum IDR (%)			Base Shear (kN)	Maximum RIDR (%)
		1st Storey	2nd Storey	3rd Storey		
X	1a	0.25	0.35	0.25	1493	0.003
	1b	0.34	0.49	0.39	1893	0.027
	2a	0.26	0.37	0.28	1416	0.005
	2b	0.25	0.36	0.29	1456	0.036
	3a	0.26	0.36	0.28	1507	0.002
	3b	0.29	0.41	0.32	1796	0.009
Y	1a	0.13	0.19	0.15	2066	0.013
	1b	0.01	0.15	0.12	1688	0.006
	2a	0.10	0.14	0.12	1613	0.009
	2b	0.14	0.21	0.18	1838	0.013
	3a	0.14	0.21	0.17	1977	0.001
	3b	0.15	0.22	0.17	1666	0.010

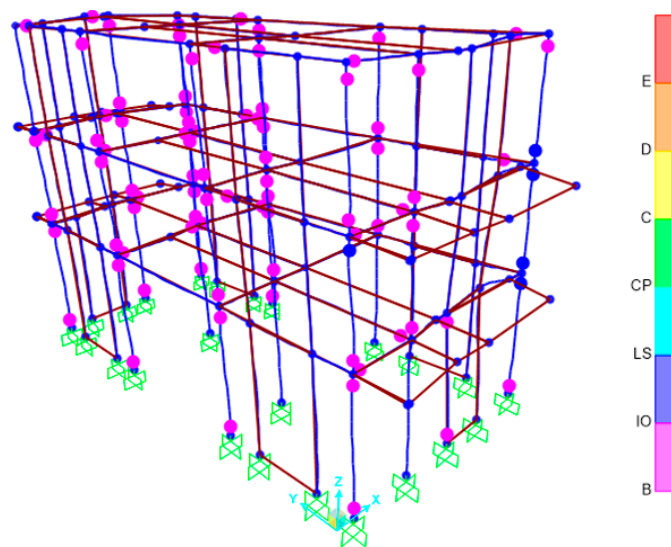


Figure 12. Plastic hinge formations—Finite Element Model (FEM).

The Von Mises stresses and the maximum shear stresses of the SPSWs are listed in Table 8, demonstrating that with respect to the model of Figure 8, the SPSWs are certainly better utilized, and one of them yields (Figure 13).

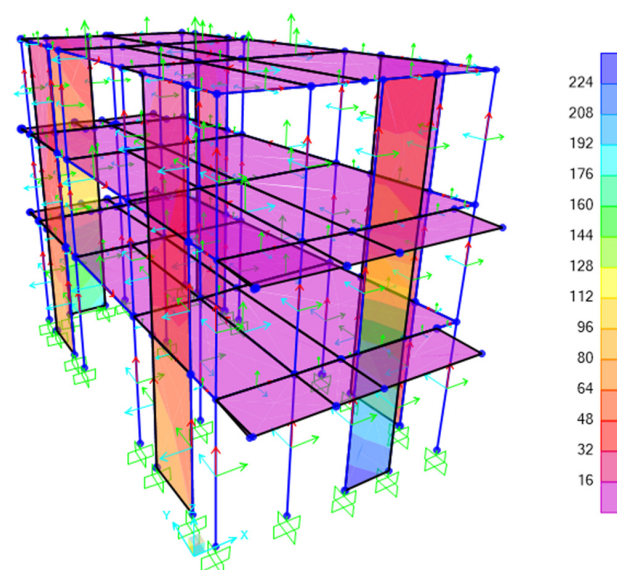


Figure 13. Von Mises stresses (in MPa) to the SPSWs—Finite Element Model (FEM).

Table 8. Maximum Von Mises and shear stress to SPSWs.

Seismic Motion	Von Mises Stress (MPa)	≤ 235 MPa	Maximum Shear Stress τ_{\max} (MPa)	$\leq 235/\sqrt{3}$ MPa
1a	136.5	✓	85.9	✓
1b	238.9	Yield	86.7	✓
2a	130.0	✓	86.8	✓
2b	90.7	✓	72.9	✓
3a	72.6	✓	79.8	✓
3b	205.6	✓	104.7	✓

5.3. Comparison of EBM and FEM

From the results presented in the two previous sections, one concludes that the modeling of SPSWs by FEM indicates the ductile behavior of the building and an increase in its lateral load capacity (in terms of base shear). On the contrary, the EBM does not lead to the expected tension-field action, as the equivalent diagonal braces do not yield even though the lateral load capacity of the building increases. Furthermore, the EBM leads to undesirable plastic hinge excursions in 4 out of 6 NLTH analyses. On the other hand, the FEM leads to undesirable plastic hinge excursions only in one NLTH analysis and only for the long configuration of SPSWs.

For ease of comparison regarding the number of plastic hinges formed and their performance classification, Tables 9–11 are provided for the worst seismic motion, “1b.” In these Tables, the reference (non-retrofitted) and the retrofitted (EBM and FEM) building models are included. In particular, for the FEM building models, i and ii are used to denote the long (Figure 8) and short (Figure 9), respectively, configuration of the SPSWs. It is also noted that the symbol B denotes almost elastic behavior, the symbols C and CP denote the collapse and collapse prevention performance levels, respectively, whereas the dash (-) denotes that no plastic hinge excursion occurs.

Table 9. Plastic hinges at the columns of the 1st storey.

1st Storey					
Column	Position	Reference Model	EBM	FEM i	FEM ii
C1	Base	IO	IO	IO	B
	Top	IO	IO	IO	B
C2	Base	IO	IO	C	-
	Top	IO	IO	C	-
C3	Base	IO	IO	IO	B
	Top	IO	IO	IO	IO
C4	Base	C	C	IO	-
	Top	IO	C	IO	-
C5	Base	IO	IO	IO	B
	Top	IO	IO	IO	B
C6	Base	IO	IO	IO	B
	Top	IO	IO	IO	B
C7	Base	IO	IO	IO	B
	Top	IO	B	IO	B
C8	Base	IO	IO	IO	B
	Top	IO	IO	IO	B
C9	Base	IO	IO	IO	B
	Top	IO	IO	IO	B
C10	Base	IO	IO	IO	B
	Top	IO	IO	IO	B

Table 9. *Cont.*

1st Storey					
Column	Position	Reference Model	EBM	FEM i	FEM ii
C11	Base	IO	IO	IO	-
	Top	IO	IO	IO	-
C12	Base	IO	IO	IO	-
	Top	IO	IO	IO	-

Table 10. Plastic hinges at the columns of the 2nd storey.

2nd Storey					
Column	Position	Reference Model	EBM	FEM i	FEM ii
C1	Base	IO	IO	IO	B
	Top	IO	IO	IO	IO
C2	Base	IO	IO	IO	B
	Top	IO	IO	IO	B
C3	Base	IO	IO	IO	IO
	Top	IO	IO	IO	IO
C4	Base	IO	IO	IO	B
	Top	IO	IO	IO	B
C5	Base	IO	IO	IO	B
	Top	IO	IO	IO	B
C6	Base	IO	IO	IO	B
	Top	IO	IO	IO	B
C7	Base	IO	B	IO	B
	Top	IO	IO	IO	B
C8	Base	IO	IO	IO	B
	Top	IO	IO	IO	B
C9	Base	IO	IO	IO	B
	Top	IO	IO	IO	B
C10	Base	IO	IO	IO	B
	Top	IO	IO	IO	B
C11	Base	IO	IO	IO	B
	Top	IO	IO	IO	B
C12	Base	IO	IO	IO	B
	Top	IO	IO	IO	B

Table 11. Plastic hinges at the columns of the 3rd storey.

3rd Storey					
Column	Position	Reference Model	EBM	FEM i	FEM ii
C1	Base	B	B	-	B
	Top	B	IO	B	B
C2	Base	B	IO	B	B
	Top	B	IO	B	B
C3	Base	-	B	-	IO
	Top	B	IO	-	B
C4	Base	B	B	-	B
	Top	B	IO	B	B

Table 11. Cont.

3rd Storey					
Column	Position	Reference Model	EBM	FEM i	FEM ii
C5	Base	B	B	B	B
	Top	B	IO	B	B
C6	Base	-	B	-	B
	Top	-	IO	-	B
C7	Base	B	B	B	B
	Top	B	C	B	B
C8	Base	-	B	-	-
	Top	-	IO	-	-
C9	Base	B	B	B	B
	Top	B	IO	B	B
C10	Base	B	B	B	B
	Top	B	IO	B	B
C11	Base	B	B	B	B
	Top	B	IO	B	B
C12	Base	B	B	B	B
	Top	B	IO	B	B

Upon inspection of Tables 9–11, it is revealed that the number of plastic hinges has been remarkably reduced in the FEM ii model (short SPSWs—Figure 9). Taking into account similar tables that can be constructed for the rest of the seismic motions but are not shown herein for space reasons, it can be said that the soft-storey mechanism anticipated in the reference (non-retrofitted) building is rather avoided.

5.4. Orthotropic Membrane Model (OMM)

This model is considered the most accurate one regarding the representation of the actual behavior of the SPSW [17]. In particular, membrane elements in conjunction with an orthotropic steel material (herein S235 is assumed) are utilized to model the SPSW.

An OMM depends on the inclination angle α , leading, thus, to a reorientation of the local axes of the area elements. Therefore, the local axes of the membrane elements are rotated by 45° . Following [17], the stiffness value along the axis that corresponds to the compression diagonal is degraded to 2%, whereas the Poisson ratio and the shear modulus are set to zero. In this way, the tension-field action of the web-plate of the SPSW is accurately represented.

The OMM is employed for the building in which small SPSWs are configured (Figure 9). Modal analysis is performed, and the fundamental period of the building is $T_1 = 0.428$ s. The maximum values from NLTH analyses for IDRs, RIDR and base shear are listed in Table 12. In comparison to the results presented for the FEM ii model in Section 5.2, the maximum RIDR increases to $0.077\% < 0.5\%$ and the maximum base shear reduces to 2011 kN (i.e., by 2.7%). The worst plastic hinge distribution obtained from the NLTH analyses (seismic motion “1b”) is shown in Figure 14. A comparison of the number of plastic hinge excursions for the FEM model in Figure 9 and the OMM model in Figure 14 reveals slightly better behavior in favor of the FEM model.

In order to evaluate the tension-field action in the OMM, the maximum Von Mises and normal stresses are listed in Table 13, where S11 and S12 correspond to tensile and compressive stresses, respectively. Figures 15 and 16 display the Von Mises stresses and principal tensile stresses, respectively, for the worst seismic motion “1b”. From the results of Table 13 and in conjunction with Figures 15 and 16, yielding of the web-plate of the SPSW is achieved, confirming the ductile behavior sought; nevertheless, the ultimate strength of 360 MPa (steel material S235) is considerably exceeded for seismic motion “1b”.

Table 12. Maximum values for IDR, RIDR, and base shear.

Horizontal Direction of the Building	Seismic Motion	Maximum IDR (%)			Base Shear (kN)	Maximum RIDR (%)
		1st Storey	2nd Storey	3rd Storey		
X	1a	0.31	0.39	0.31	1252	0.009
	1b	0.48	0.64	0.46	1901	0.006
	2a	0.30	0.37	0.26	1391	0.013
	2b	0.28	0.37	0.28	1083	0.077
	3a	0.30	0.42	0.32	1275	0.012
	3b	0.34	0.46	0.35	1483	0.039
Y	1a	0.19	0.25	0.18	1977	0.023
	1b	0.16	0.21	0.15	1754	0.007
	2a	0.15	0.19	0.15	1582	0.007
	2b	0.18	0.24	0.17	1615	0.014
	3a	0.21	0.25	0.16	2011	0.005
	3b	0.19	0.24	0.17	1601	0.011

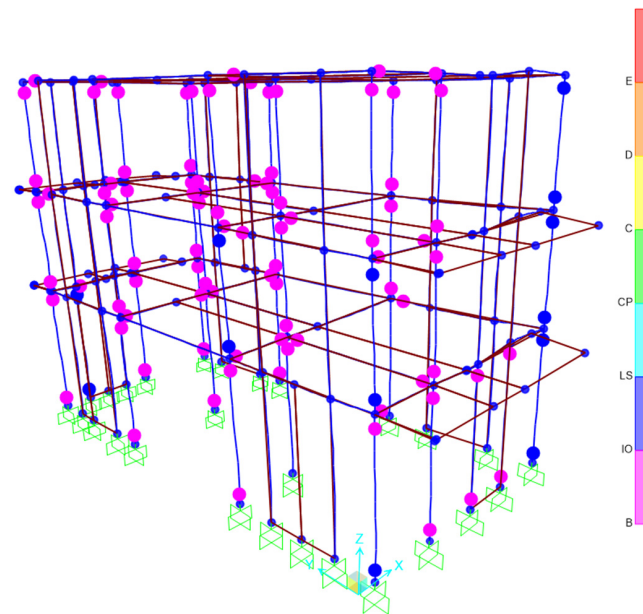


Figure 14. Plastic hinge formations—Orthotropic Membrane Model (OMM).

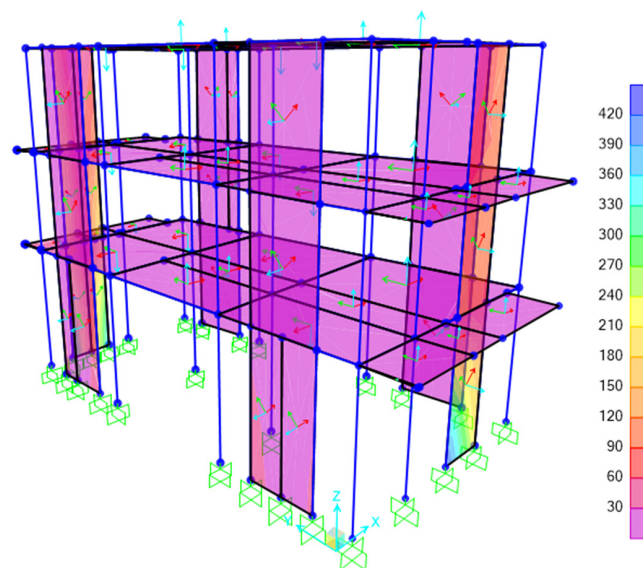


Figure 15. Von Mises stresses (in MPa) to the SPSWs—Orthotropic Membrane Model (OMM).

Table 13. Maximum Von Mises and principal stress to SPSWs, status of the SPSW.

Seismic Motion	Von Mises Stress	Status	S11 (MPa)	S22 (MPa)
1a	155.0	Yield	263.9	5.8
1b	436.2	Yield/Fail	355.9	8.9
2a	157.7	Yield	249.2	5.8
2b	132.0	Yield	247.2	6.1
3a	208.1	Not yield	206.5	5.6
3b	299.1	Yield	297.6	7.7

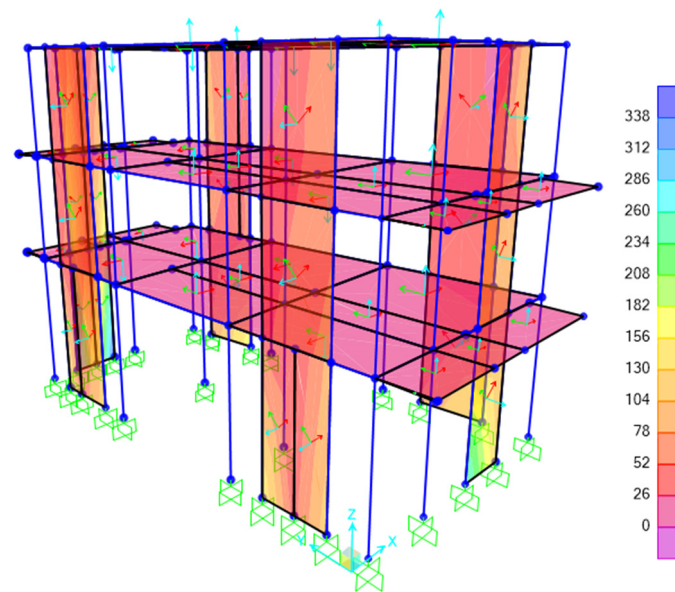


Figure 16. Principal tensile stresses S11 (in MPa)—Orthotropic Membrane Model (OMM).

To ensure that the ultimate strength of the web-plates of the SPSW is not exceeded, the NLTH analyses are repeated, assuming the thickness t of the web-plate for all SPSWs to be 9.0 mm. Modal analysis is performed, and the fundamental period of the building is now $T_1 = 0.406$ s. The maximum values from NLTH analyses for IDRs, RIDR and base shear are presented in Table 14 and are compared with those of Table 12. One easily notices that the maximum RIDR increases to $0.093\% < 0.5\%$, and the maximum base shear also increases to 2202 kN (i.e., by 9.5%).

Table 14. Interstorey drift ratios and base shear forces.

Horizontal Direction of the Building	Seismic Motion	Maximum IDR (%)			Base Shear (kN)	Maximum RIDR (%)
		1st Storey	2nd Storey	3rd Storey		
X	1a	0.27	0.39	0.31	1318	0.018
	1b	0.40	0.61	0.49	1813	0.020
	2a	0.28	0.39	0.27	1461	0.016
	2b	0.25	0.38	0.31	1172	0.093
	3a	0.29	0.44	0.36	1426	0.025
	3b	0.32	0.49	0.39	1505	0.027
Y	1a	0.17	0.24	0.19	2101	0.021
	1b	0.13	0.19	0.14	1596	0.010
	2a	0.13	0.18	0.12	1596	0.010
	2b	0.16	0.25	0.20	1646	0.015
	3a	0.18	0.25	0.18	2202	0.010
	3b	0.17	0.25	0.19	1733	0.021

Figure 17 displays the worst plastic hinge distribution obtained from the NLTH analyses (seismic motion “1b”). A comparison of the number of plastic hinge excursions in Figures 14 and 17 reveals that the increase in thickness from 5.0 to 9.0 mm leads to slightly better behavior. If plastic hinge excursions for the rest of seismic motions are compared (the corresponding figures are not shown herein for space reasons), one concludes that this increase in thickness certainly improves the behavior of the building and, in all likelihood, the exhibition of a soft-storey mechanism is avoided.

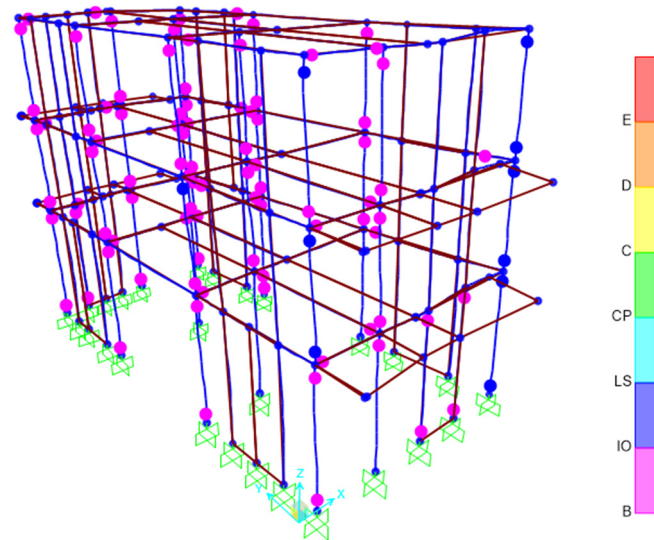


Figure 17. Plastic hinge formations—Orthotropic Membrane Model (OMM), $t = 9.0$ mm.

The maximum Von Mises and normal (tensile and compressive) stresses are listed in Table 15, whereas Figures 18 and 19 display the Von Mises stresses and principal tensile stresses, respectively, for the worst seismic motion “1b”. From the results of Table 15 and in conjunction with Figures 18 and 19, yielding of the web-plate of the SPSW is now achieved for three seismic motions, but the ultimate strength of 360 MPa is not exceeded. Therefore, the desired behavior of the retrofitted SPSWs r/c building is obtained for all seismic motions considered.

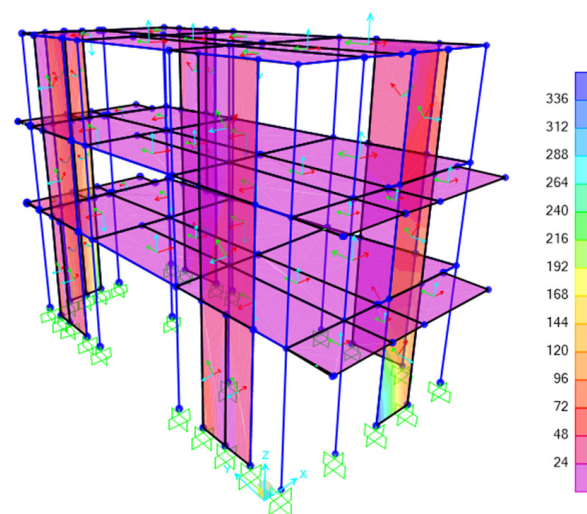
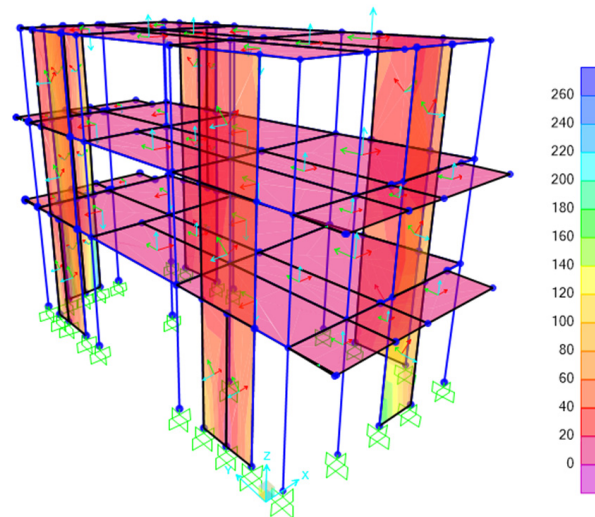


Figure 18. Von Mises stresses (in MPa) to the SPSWs—Orthotropic Membrane Model (OMM), $t = 9.0$ mm.

Table 15. Maximum Von Mises and principal stress to SPSWs, status of the SPSW.

Seismic Motion	Von Mises Stress	Status	S11 (MPa)	S22 (MPa)
1a	126.0	Not yield	221.7	4.6
1b	350.7	Yield	272.4	6.6
2a	110.5	Yield	239.1	4.7
2b	124.3	Not yield	211.0	3.9
3a	158.2	Not yield	229.9	4.8
3b	196.8	Yield	247.2	6.2

**Figure 19.** Principal tensile stresses S11 (in MPa)—Orthotropic Membrane Model (OMM), $t = 9.0$ mm.

Taking into account that for the seismic retrofit of existing r/c buildings in seismic regions, energy dissipation is sought [2,3], the SPSW should be designed to yield but not fail. On the other hand, if only added stiffness and/or strength are required for seismic retrofit purposes, then yielding of the SPSW is not allowed, keeping in mind that the thickness of the SPSW depends on the geometric properties of the VBEs and HBEs [13,14,17].

6. Conclusions

This paper investigates the seismic retrofit and upgrade of an existing r/c building using SPSWs. SPSWs are able to provide both stiffness and ductility; however, their actual behavior has to be appropriately represented in the numerical model. Additionally, the placement and configuration of the SPSWs is a critical factor concerning their contribution to the anticipated seismic performance of the building.

Three different options are utilized herein to model SPSWs, and the seismic performance of the retrofitted r/c building is assessed by a number of NLTH analyses. From the results of these analyses, in terms of specific seismic response indices and plastic hinge formations to the members of the building, it is concluded that short-length SPSWs in conjunction with an orthotropic membrane model (OMM) for them provide the best option. As an alternative good option, one may select a finite element model (FEM) instead of the OMM; on the other hand, the equivalent brace model (EBM) is not recommended. Taking into account that discretization by membrane elements in conjunction with orthotropic material properties are common options in all modern structural analysis software, the implementation of an OMM for the SPSW is easy and leads to accurate response results.

The retrofitted SPSWs r/c building under study exhibits desirable transient and residual interstorey drift characteristics, as well as a substantial increase in base shear and energy dissipation capacity. As a general conclusion and essentially a final suggestion to be made, in the imminent or future revision of modern seismic retrofit codes [3,35], the option of utilizing SPSWs for seismic upgrading purposes of existing r/c buildings should be

added. In this sense, both the FEM and OMM options for modeling SPSW can be proposed; nevertheless, the OMM option may be preferred because it represents the tension-field action of the SPSW better than the FEM option. Obviously, the final decision with respect to the configuration of the SPSW strongly depends on the r/c building to be retrofitted.

Author Contributions: Conceptualization, N.B. and G.P.; Methodology, N.B. and G.P.; Software, N.B. and G.P.; Supervision, G.P.; Validation, N.B. and G.P.; Writing—original draft, N.B. and G.P.; Writing—review & editing, G.P. All authors have read and agreed to the published version of the manuscript.

Funding: This research received no external funding.

Institutional Review Board Statement: Not applicable.

Informed Consent Statement: Not applicable.

Data Availability Statement: The data that support the findings of this study are available from the authors upon reasonable request.

Conflicts of Interest: The authors declare no conflict of interest.

References

1. Royal Decree Code for Seismic Resistance (R.D.) of 19/26.2.1959 (FEK 36/A); About the Code for Seismic Resistance of Buildings; Earthquake Planning & Protection Organization: Athens, Greece, 1959.
2. Antoniou, S. *Seismic Retrofit of Existing Reinforced Concrete Buildings*; Wiley Blackwell: Hoboken, NJ, USA, 2023.
3. Eurocode 8 (EC8). *Design of Structures for Earthquake Resistance—Part 1–3: Assessment and Retrofitting of Buildings*; European Committee for Standardization (CEN): Brussels, Belgium, 2010.
4. Mahrenholtz, C.; Lin, P.-C.; Wu, A.-C.; Tsai, K.-C.; Hwang, S.-J.; Lin, R.-Y.; Bhayusukma, M.Y. Retrofit of reinforced concrete frames with buckling-restrained braces. *Earthq. Eng. Struct. Dyn.* **2015**, *44*, 59–78. [[CrossRef](#)]
5. Qu, Z.; Kishiki, S.; Maida, Y.; Sakata, H.; Wada, A. Seismic response of reinforced concrete frames with buckling restrained braces in zigzag configuration. *Eng. Struct.* **2015**, *105*, 12–21. [[CrossRef](#)]
6. Pan, K.-Y.; Wu, A.-C.; Tsai, K.-C.; Li, C.-H.; Khoo, H.-H. Seismic retrofit of reinforced concrete frames using buckling restrained braces with bearing block load transfer mechanism. *Earthq. Eng. Struct. Dyn.* **2016**, *45*, 2303–2326. [[CrossRef](#)]
7. Barbagallo, F.; Boscp, M.; Marino, E.M.; Rossi, P.P.; Stramondo, P.R. A multi-performance design method for seismic upgrading of existing RC frames by BRBs. *Earthq. Eng. Struct. Dyn.* **2017**, *46*, 1099–1119. [[CrossRef](#)]
8. Castaldo, P.; Tubaldi, E.; Selvi, F.; Gioiella, L. Seismic performance of an existing RC structure retrofitted with buckling restrained braces. *J. Build. Eng.* **2021**, *33*, 101688. [[CrossRef](#)]
9. Tsarpalis, P.; Vayas, I.; Thanopoulos, P.; Vamvatsikos, D. Rehabilitation of reinforced concrete building using the fuseis beam-link system. *Structures* **2021**, *34*, 3300–3314. [[CrossRef](#)]
10. Di Lorenzo, G.; Tartaglia, R.; Prota, A.; Landolfo, R. Design procedure for orthogonal steel exoskeleton structures for seismic strengthening. *Eng. Struct.* **2023**, *275*, 115252. [[CrossRef](#)]
11. Jung, J.-S.; Lee, B.-G.; Lee, K.-S. Seismic capacity of exiting reinforced concrete buildings strengthened with a novel prestressing steel frame system for increasing lateral strength. *J. Build. Eng.* **2023**, *79*, 107856. [[CrossRef](#)]
12. Katsimpini, P.; Papagiannopoulos, G. Effectiveness of the seesaw system as a means of seismic upgrading in older, non-ductile reinforced concrete buildings. *Vibration* **2023**, *6*, 102–242. [[CrossRef](#)]
13. *ANSI/AISC 341-22; Seismic Provisions for Structural Steel Buildings*. American Institute of Steel Construction: Chicago, IL, USA, 2022.
14. *CSA S16-19; Design of Steel Structures*. Canadian Standards Association: Toronto, ON, Canada, 2009.
15. Baldelli, J.A., Jr. Steel Shear Walls for Existing Buildings. *Eng. J.* **1983**, *20*, 70–77.
16. Thorburn, L.J.; Kulak, J.G.; Montgomery, C. *Analysis of Steel Plate Shear Walls, Structural Engineering Report No.107*; Department of Civil Engineering, The University of Alberta: Edmonton, AB, Canada, 1983.
17. Sabelli, R.; Bruneau, M. *Steel Design Guide 20—Steel Plate Shear Walls*; American Institute of Steel Construction: Chicago, IL, USA, 2006.
18. De Matteis, G.; Formisano, A.; Mazzolani, F.M. An innovative methodology for seismic retrofitting of existing RC buildings by metal shear panels. *Earthq. Eng. Struct. Dyn.* **2009**, *38*, 61–78. [[CrossRef](#)]
19. Choi, I.-R.; Park, H.-G. Cyclic loading test for reinforced concrete frame with thin steel infill plate. *J. Struct. Eng.* **2011**, *137*, 654–664. [[CrossRef](#)]
20. Formisano, A.; Lombardi, L.; Mazzolani, F.M. Perforated metal shear panels as bracing devices of seismic-resistant structures. *J. Constr. Steel Res.* **2016**, *126*, 37–49. [[CrossRef](#)]
21. Formisano, A.; Lombardi, L. Low yield metals and perforated steel shear walls for seismic protection of existing RC buildings. *Cogent Eng.* **2018**, *5*, 1525813. [[CrossRef](#)]

22. Bypour, M.; Gholhaki, M.; Kioumarsi, M.; Kioumarsi, B. Nonlinear analysis to investigate effect of connection type on behavior of steel plate shear wall in RC frame. *Eng. Struct.* **2019**, *179*, 611–624. [[CrossRef](#)]
23. Parvizi, M.; Fathi, M.; Zamani, S.S.M.; Shakib, H. Experimental and numerical study of concrete frames with steel plate shear walls. *J. Constr. Steel Res.* **2022**, *196*, 107404. [[CrossRef](#)]
24. Astaneh-Asl, A. *Seismic Behavior and Design of Steel Shear Walls—Steel Tip 37*; Structural Steel Educational Council: Moraga, CA, USA, 2001.
25. Berman, J.W. Seismic behavior of code designed steel plate shear walls. *Eng. Struct.* **2011**, *33*, 230–244. [[CrossRef](#)]
26. Yang, Y.; Feng, S.; Xue, Y.; Yu, Y.; Wang, H.; Chen, Y. Experimental study on shear behavior of fire-damaged reinforced concrete T-beams retrofitted with prestressed steel straps. *Constr. Build. Mater.* **2019**, *209*, 644–654. [[CrossRef](#)]
27. Markou, G. A new method of seismic retrofitting cost analysis and effectiveness for reinforced concrete structures. *Eng. Struct.* **2021**, *246*, 113083. [[CrossRef](#)]
28. Szép, J.; Habashneh, M.; Lógó, J.; Movahedi Rad, M. Reliability Assessment of Reinforced Concrete Beams under Elevated Temperatures: A Probabilistic Approach Using Finite Element and Physical Models. *Sustainability* **2023**, *15*, 6077. [[CrossRef](#)]
29. SAP2000. *Integrated Software for Structural Analysis & Design*; Computers and Structures Inc.: Berkeley, CA, USA, 2023.
30. Eurocode 8 (EC8). *Design of Structures for Earthquake Resistance—Part 1: General Rules, Seismic Actions and Rules for Buildings*; European Committee for Standardization (CEN): Brussels, Belgium, 2004.
31. EAK 2000. *EAK 2000 Greek Seismic Code*; Earthquake Planning and Protection Organization of Greece: Athens, Greece, 2000.
32. ASCE 41-17; Seismic Evaluation and Retrofit of Existing Buildings. American Society of Civil Engineers: Reston, VA, USA, 2017.
33. Sucuoğlu, H.; Akkar, S. *Basic Earthquake Engineering*; Springer: Cham, Switzerland, 2014.
34. McCormick, J.; Aburano, H.; Ikenaga, M.; Nakashima, M. Permissible residual deformation levels for building structures considering both safety and human elements. In Proceedings of the 14th World Conference on Earthquake Engineering, Beijing, China, 12–17 October 2008.
35. KAN.EPE. *Code of Structural Interventions—FEK_3197_B_22_6_2022*; Earthquake Planning and Protection Organization of Greece: Athens, Greece, 2022.

Disclaimer/Publisher’s Note: The statements, opinions and data contained in all publications are solely those of the individual author(s) and contributor(s) and not of MDPI and/or the editor(s). MDPI and/or the editor(s) disclaim responsibility for any injury to people or property resulting from any ideas, methods, instructions or products referred to in the content.